

Phonon Scattering Engineered Unconventional Thermal Radiation at the Nanoscale

Dudong Feng, Xiaolong Yang, and Xiulin Ruan*



Cite This: <https://doi.org/10.1021/acs.nanolett.3c03375>



Read Online

ACCESS |



Metrics & More



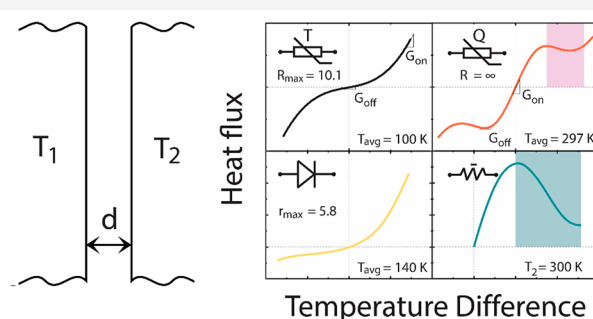
Article Recommendations



Supporting Information

ABSTRACT: We show that engineering phonon scattering, such as through isotope enrichment and temperature modulation, offers the potential to achieve unconventional radiative heat transfer between two boron arsenide bulks at the nanoscale, which holds promise in applications for nonlinear thermal circuit components. A heat flux regulator is proposed, where the temperature window for stabilized heat flux exhibits a wide tunability through phonon scattering engineering. Additionally, we propose several other nonlinear thermal radiative devices, including a negative differential thermal conductance device, a temperature regulator, and a thermal diode, all benefiting from the design space enabled by isotope and temperature engineering of the phonon linewidth. Our work highlights the capability of temperature and isotope engineering in designing and optimizing nonlinear radiative thermal devices and demonstrates the potential of phonon engineering in thermal radiative transport.

KEYWORDS: Isotope engineering, Negative differential thermal conductance, Heat flux regulator, Near-field radiation, Phonon linewidth, Surface phonon-polaritons



Nonlinear heat transfer, in contrast to conventional heat transfer, represents a phenomenon where the heat flux does not exhibit a linear dependence on the temperature difference between two reservoirs.¹ It serves as the underlying mechanism for various nonlinear thermal circuit components,¹ including thermal switches,^{2–4} thermal diodes,^{5–9} thermal regulators,^{10–12} and negative differential thermal conductance (NDTC) devices.^{5,13–15} Similar to their electronic counterparts, nonlinear thermal circuits can potentially enable diverse applications such as renewable energy conversion and harvesting,^{3,16,17} thermal energy storage,¹⁸ personal and building thermal comfort,^{10,19–21} spacecraft thermal management,^{22,23} and cooling of electronic devices and data centers.^{24,25} Developing high-performance nonlinear thermal components holds significant potential in tackling global challenges such as the climate crisis, energy shortages, carbon emissions, and environmental pollution.

While nonlinear heat transfer naturally occurs in boiling and convection processes, research investigations into these solid-state nonlinear thermal devices through conduction and radiation began this century. NDTC refers to a nonlinear thermal transport phenomenon where heat flow decreases as the temperature difference increases, i.e., $(\partial Q_{1 \rightarrow 2} / \partial T_1)|_{T_2}$ or $(-\partial Q_{1 \rightarrow 2} / \partial T_2)|_{T_1}$ is negative.^{13,14} Here, T_1 and T_2 represent the temperatures of hot and cold terminals, respectively. Conduction-based NDTC concept was initially proposed by Li et al.,¹³ while thermal radiation-based NDTC was later

theoretically proposed by Zhu et al.,¹⁴ where NDTC is achieved by coupling/decoupling surface phonon-polaritons (SPhPs) at near-field regime when the hot terminal temperature increases. Inspired by this temperature-dependent dielectric functions of SiC, researchers employ optical phase change materials (PCMs) or complex geometric design, along with near-field electromagnetic theory, to achieve strong NDTC across a nanoscale vacuum spacing.^{26,27}

Thermal regulator and thermal diode are fundamental components of nonlinear thermal circuits, and they can be realized using either conduction or radiation to control thermal transport while maintaining the solid-state condition.¹ Compared to conduction-based nonlinear thermal devices,^{8,28,29} radiative thermal regulators and diodes tend to offer better performance due to the inherent nonlinearity of radiative heat transfer.¹ The performance of a thermal regulator is characterized by its on/off switching ratio, i.e., $R = G_{\text{on}}/G_{\text{off}}$, where $G = dQ/d(\Delta T)$ is the differential thermal conductance. A thermal diode is assessed based on its rectification ratio, i.e., $r = q_f/q_r - 1$. Complex surface or

Received: September 5, 2023

Revised: October 22, 2023

Accepted: October 23, 2023

layered nanostructures and PCMs are commonly utilized in the implementation of radiative thermal regulation and thermal diode functionalities both theoretically^{30–33} and experimentally.^{34–36} However, these approaches have limitations such as the fabrication complexity of nanostructures and the fixed working temperature determined by the critical temperature of PCMs. Few studies have shown satisfactory performance without relying on PCMs or nanostructures.³⁷ Therefore, it is crucial to develop nonlinear thermal components with tunable working conditions that offer greater design flexibility for nonlinear thermal circuits.

Recently, phonon scattering science, including three-phonon³⁸ and four-phonon scattering,^{39–42} on infrared and Raman spectra has attracted significant attention. Isotope scattering, as another phonon scattering mechanism, also emerged as a fascinating area of research for modulating diverse material properties.^{43–48} Dominated by coupled SPhPs, near-field radiative heat transfer between polar dielectrics could be actively tuned by isotopically engineered phonon linewidth.^{49,50} Naturally, the technique of isotope engineering has been employed to enhance the performance of near-field radiative thermal diodes.⁵¹ In this Letter, we investigate the potential of isotope engineering to control near-field radiative heat transfer between two boron arsenide (BAs) semi-infinite solids. Our study theoretically demonstrates a radiative heat flux regulator with infinite switching ratio by leveraging the temperature-dependent phonon linewidth combined with near-field radiation. Furthermore, we achieve a range of nonlinear radiative transfer devices, including NDTC devices and temperature thermal regulators. By adjusting the isotope concentrations, we can tune the operating temperature of the NDTC device and the temperature window for stabilized heat flux of the heat flux regulators. Moreover, by introducing asymmetry in the isotope composition of one of the terminals, we created a radiative thermal diode. This innovative and rich approach to nonlinear radiative transfer through phonon scattering engineering opens up exciting possibilities for the development of thermal circuit components, significantly expanding the interdisciplinary applications of conduction and radiation.

As shown in Figure 1a, the nonlinear radiative thermal device requires two bodies at thermal equilibrium (T_1 and T_2) separated by a small vacuum gap, which can leverage the feature of near-field radiation mediated by SPhPs. BAs is selected as the terminal material due to its strong temperature-dependent optical response. The temperature-dependent

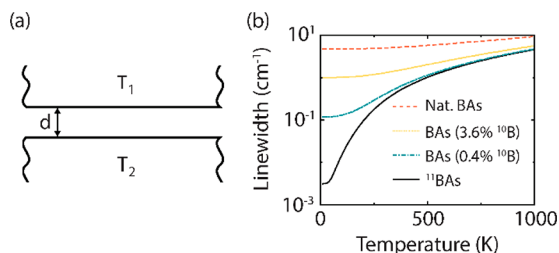


Figure 1. Schematic diagram and material property of the nonlinear radiative thermal devices. (a) All presented devices consist of two BAs semi-infinite solids separated by a vacuum gap of distance d . The hot and cold terminal temperatures are set at T_1 and T_2 , respectively. (b) Phonon linewidth of BAs as a function of temperature with different isotope concentrations of boron.

dielectric function of BAs is given by Lorentz oscillator model:⁵²

$$\epsilon(\omega, T) = \epsilon_{\infty} \left(1 + \frac{\omega_{LO}^2 - \omega_{TO}^2}{\omega_{TO}^2 - \omega^2 - i\omega\gamma(T)} \right) \quad (1)$$

where ϵ_{∞} is the dielectric constant at the high-frequency limit, and ω is the photon frequency. $\omega_{TO} = 681.5 \text{ cm}^{-1}$ (20.4 THz) and $\omega_{LO} = 684.7 \text{ cm}^{-1}$ (20.5 THz) represent the transverse and longitudinal optical phonon frequencies, respectively, which are assumed to be temperature insensitive. γ is the temperature-dependent phonon line width, which can be obtained from first-principles calculations:³⁹

$$\gamma(T) = \gamma_{ph}(T) + \gamma_{iso}(T) \quad (2)$$

where T is the material temperature at thermal equilibrium. The subscripts ph and iso indicate the contributions from phonon scattering and isotope effect, respectively. The optical phonon frequencies and phonon line width are obtained from first-principles calculations. As intensively discussed in previous literature,^{39,53} the corresponding calculation method would not be addressed here.

Figure 1b shows the temperature-dependent phonon linewidth of BAs at different isotope concentrations of boron. Due to increased significance of four-phonon scattering at high temperature,^{39,54,55} the phonon linewidth of BAs exhibits a strong temperature dependence, potentially leading to a significant nonlinear impact on the radiative heat flux. Additionally, alterations in the isotope concentration of elements can substantially tune the phonon linewidth due to changes in the average mass.⁵⁶ Notably, as the isotope concentration of ^{10}B increases from 0 to 19.8%, the phonon linewidth undergoes significant changes spanning several orders of magnitude below 500 K. This observation presents a large design space for the development of potential nonlinear thermal devices with enhanced performance.

The dielectric functions of BAs around Reststrahlen band ($\omega_{TO} < \omega < \omega_{LO}$) at 200 and 600 K are shown in Figure 2. A

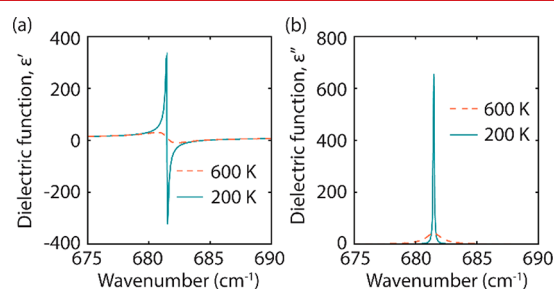


Figure 2. Temperature-dependent dielectric functions of BAs. (a) The real and (b) imaginary parts of the dielectric function of isotopically pure BAs at 200 and 600 K. The corresponding phonon linewidths at 200 and 600 K are 0.10 and 1.55 cm^{-1} , respectively.

small linewidth usually indicates less friction of this vibration mode and therefore a larger oscillation at the resonance frequency. It is evident from both Figure 2a,b that there is a larger oscillation of the dielectric functions at 200 K compared to 600 K. As shown in Figure 2b, the imaginary parts of the dielectric function of BAs usually correspond to the absorption capability of near-field radiative heat transfer. Therefore, the dielectric function at 200 K implies a potentially higher absorption peak at the resonance frequency than that at 600 K.

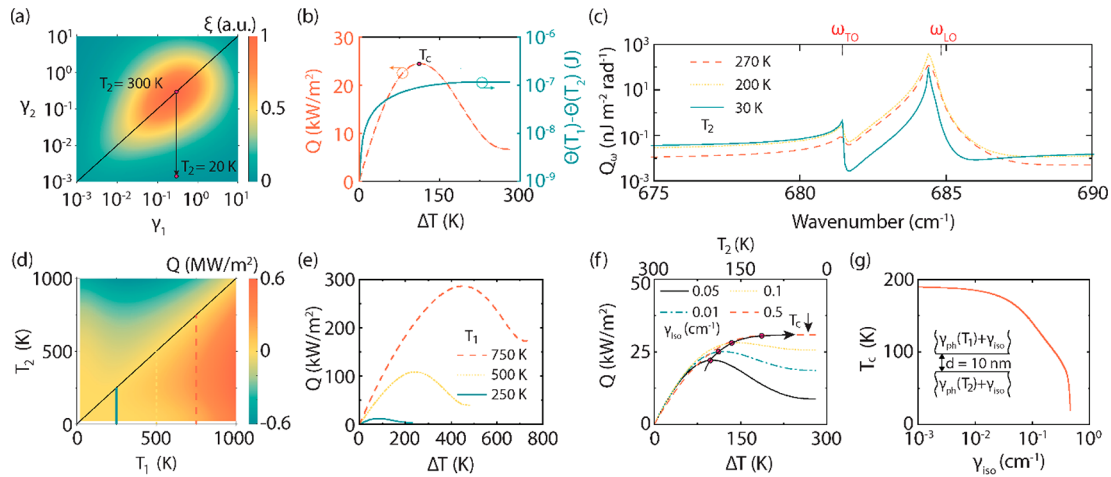


Figure 3. Schematic and mechanism of an NDTC device. (a) Contour plot of the normalized spectral integration of the energy transmission coefficient as a function of phonon linewidths of both terminals. (b) Radiative heat flux between two BAs semi-infinite solids (left axis) and spectral integration of the energy difference between two Planck oscillators (right axis) as a function of temperature difference. (c) Spectral heat fluxes between two BAs semi-infinite solids with different cold terminal temperatures. Note that the hot terminal temperature is always fixed at 300 K for (a–c), and the vacuum spacing is fixed at 10 nm unless specifically mentioned. (d) Contour plot of radiative heat flux with respect to the temperatures of hot and cold terminals. (e) Radiative heat flux with respect to temperature difference at different hot terminal temperatures. (f) Radiative heat flux with respect to cold terminal temperature for different isotope treatments. (g) Critical temperature as a function of isotope phonon linewidth. Note that isotope engineering is applied to both terminals and $\Delta T = T_1 - T_2$. By default, BAs semi-infinite solids are assumed to be isotopically pure ^{11}BAs unless stated otherwise.

However, the full width at the half-maximum of the absorption peak at 600 K should be larger than that at 200 K. This trade-off phenomenon potentially implies an optimal linewidth to achieve the maximum near-field radiative flux at a given temperature difference.^{50,53}

A fluctuational electrodynamics formalism is applied to calculate the net radiative heat flux between the two semi-infinite solids.⁵² The spectral heat flux per unit area is calculated by

$$Q_\omega = \frac{1}{4\pi^2} \int_0^\infty [\Theta(\omega, T_1) - \Theta(\omega, T_2)] \xi(\omega) \quad (3)$$

where $\Theta(\omega, T) = \hbar\omega[\exp(\hbar\omega/k_B T) - 1]^{-1}$ is the mean energy of a Planck oscillator at an angular frequency ω with \hbar and k_B being the reduced Planck constant and Boltzmann constant, respectively. $\xi(\omega)$ is the angle integration of energy transmission coefficients.⁵²

To elucidate the mechanism of NDTC in this configuration, it is essential to discuss two factors, the energy transmission coefficient, and the mean energy difference of two Planck oscillators, individually in order to calculate the net spectral heat flux as described in eq 3. Figure 3a presents a contour map of the total energy transmission coefficient ($\xi = \int_0^\infty \xi(\omega) d\omega$) while varying the phonon linewidths on both terminals from 10^{-3} cm^{-1} to 10 cm^{-1} . The hot spot observed in the contour plot indicates the existence of an optimal phonon linewidth pair that can provide with the maximum energy transmission probability between two BAs semi-infinite solids. When the phonon linewidths of both terminals approach each other, the total energy transmission probability increases. By drawing a vertical line on the contour map and varying γ_2 from $T_2 = 300 \text{ K}$ to $T_2 = 20 \text{ K}$, it becomes evident that the capability of near-field radiative heat transfer weakens as the temperature difference increases. However, Figure 3b illustrates that the mean energy difference of the two Planck oscillators increases continuously as the temperature difference rises. Taking into

account the combined effect of these two factors, the net radiative heat flux initially increases as the temperature difference rises. Nonetheless, once the temperature exceeds the critical temperature ($T_c = 190 \text{ K}$), the reduction in the near-field energy transmission coefficient becomes the dominant factor, leading to a decrease in the net radiative heat flux. As a result, the NDTC feature is achieved within the temperature range of 190 to 20 K.

The spectral heat flux analysis reveals important details about NDTC behavior. Figure 3c shows that when T_2 is 200 K, the spectral heat flux is the highest compared to T_2 values of 270 and 30 K. At 30 K, the limited contribution from coupled SPhPs within the Reststrahlen band leads to a lower total heat flux. Similarly, at 270 K, the spectral heat flux outside the Reststrahlen band decreases significantly due to a smaller temperature difference, resulting in a lower total heat flux. This observation explains the mechanism of NDTC in the near-field energy exchange between two BAs semi-infinite solids.

To investigate the NDTC behavior across a wide temperature range, we present a contour plot of the radiative heat flux with the temperatures of both the hot and cold terminals varying from 20 to 1000 K. As shown in Figure 3d, the radiative heat flux exhibits a symmetric distribution along the diagonal, indicating the geometric symmetry of the two-terminal configuration. Remarkably, NDTC behavior is observed across all hot terminal temperatures. To further demonstrate this, Figure 3e highlights the NDTC behavior for three selected temperatures. The critical temperatures for these cases are 83, 243, and 451 K, corresponding to increasing hot terminal temperatures of 250, 500, and 750 K, respectively. By tuning the temperature of the hot terminal in this configuration, we can effectively adjust the range of NDTC behavior. This flexibility allows for precise control and customization of the desired temperature range for NDTC applications.

Furthermore, isotope engineering can tune the material properties and the behavior of near-field radiative heat transfer

in the NDTC device. By enriching the isotopic boron in both BAs terminals (shown in Figure 3g), the phonon linewidth can be increased, leading to a smaller absolute value of NDTC and a decrease in the critical temperature with increasing γ_{iso} , as shown in Figure 3f. Additionally, Figure 3g illustrates that the manipulation of the isotope concentration in BAs enables the design flexibility of the critical temperature from 190 to 20 K, where the NDTC phenomenon disappears. This highlights the potential of isotope phonon engineering as a promising approach to control both the value and effective temperature range of NDTC devices.

Analogous to current and voltage regulators in electric circuits, thermal regulators can also be categorized into two types: temperature regulators and heat flux regulators. Figure 4a presents a temperature regulator utilizing the same

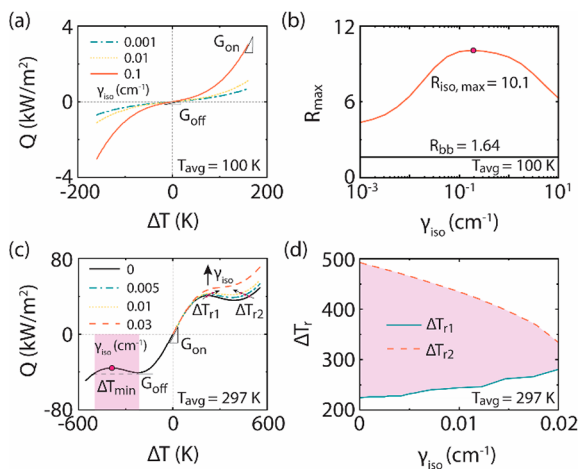


Figure 4. Isotope effect on the performance of a temperature and heat flux regulator. (a) Q – ΔT curves of a temperature regulator at different isotope concentrations. (b) Maximum switching ratio with respect to the photon linewidth due to isotope effect. The average temperature ($T_{\text{avg}} = (T_1 + T_2)/2$) of this temperature regulator is fixed at 100 K. (c) Q – ΔT curves of a heat flux regulator at different isotope concentrations. Since the Q – ΔT curve exhibits symmetry, the negative portions of the three isotope-engineered cases are omitted for clarity. The shadow area represents the temperature window for stabilized heat flux. (d) The temperature window for stabilized heat flux with respect to the phonon linewidth due to isotope effect in the heat flux regulator. The average temperature of this heat flux regulator is fixed at 297 K.

geometric structures and materials as those shown in Figure 1a. Three heat flux and temperature difference (Q – ΔT) curves are plotted to depict the performance of the temperature regulator, showcasing the impact of the isotope concentrations in both terminals. Taking the case of $\gamma_{\text{iso}} = 0.1$ cm⁻¹ as an example, the Q – ΔT curve demonstrates a strong nonlinear relationship, where the differential thermal conductance is almost 10 times lower at $\Delta T = 0$ K ($G_{\text{off}} = 4.5$ W/K m²) compared to $\Delta T = 160$ K ($G_{\text{on}} = 44.7$ W/K m²). Based on Figure 3a, the observed strong nonlinear phenomenon can be attributed primarily to the mean energy difference between the two Planck oscillators, as the transmission coefficient remains relatively stable when an isotope phonon linewidth is introduced as the baseline. In other words, when the temperature varies from 20 to 180 K, the phonon linewidth of BAs only shows a small variation from 0.10 to 0.15 cm⁻¹, resulting in even a slight increase in the energy transmission

coefficient as the temperature difference increases. By tuning the isotope concentration, the maximum on/off switching ratio can exceed 10, as depicted in Figure 4b. This value is nearly 6 times higher than that achieved using two blackbodies with the same temperature difference. The remarkable enhancement demonstrates the powerful capability of isotope engineering in significantly improving the performance of a temperature regulator.

Compared to a temperature regulator, achieving a radiative heat flux regulator is challenging at the far-field regime because the relationship between the heat flux and the temperature difference follows a fourth power function (T^4). By leveraging the combined effect of phonon linewidth matching between two BAs semi-infinite solids and temperature difference, here we propose a heat flux regulator with infinite switching ratio ($G_{\text{off}} = 0$) through near-field radiation, as shown in Figure 4c. It is worth noting that G is defined as small-signal thermal conductance, and it is important to clarify that the large-signal thermal conductance ($Q/\Delta T$) is not equal to 0 in this context. Similar to the mechanism of NDTC, the radiative heat flux initially increases with the temperature difference. However, once the temperature difference surpasses the critical temperature difference (ΔT_{r1}), the decrease in the energy transmission coefficient becomes the main factor contributing to the reduction in heat flux when $\Delta T_{r1} < \Delta T < \Delta T_{\text{min}}$. However, when the temperature difference exceeds ΔT_{min} , the energy transmission coefficient reaches a saturation value. At this point, the mean energy difference between two Planck oscillators becomes the dominant factor influencing the heat flux, leading to an increase in the radiative heat flux. As shown by the shaded area in Figure 4c, the temperature window for stabilized heat flux is bounded by ΔT_{r1} and ΔT_{r2} , where the radiative heat fluxes at these two points remains the identical. Same as the temperature regulator, the nonlinear Q – ΔT curve can be tuned by isotope engineering. As depicted in Figure 4d, by increasing the isotope concentration, ΔT_{r1} decreases from 493 to 319 K, and the temperature window for stabilized heat flux decreases from 269 to 0 K. By utilizing isotope engineering, it becomes possible to manually select the desired temperature window for stabilized heat flux based on the required temperature sensitivity. The proposal of this heat flux regulator with infinite switching ratio addresses a significant gap in nonlinear thermal circuits, offering promising prospects for advancements in thermal management and modulation.

The original symmetric schematic depicted in Figure 1a lacks the capability to function as a thermal diode due to its symmetric geometry and material properties. However, by introducing an asymmetric isotope effect in one terminal of the device, a thermal diode can be achieved, as shown in Figure 5a. The Q – ΔT curve of a thermal diode mimics the current–voltage curve of a diode, exhibiting an exponential relationship between the heat flux and temperature difference. For the forward bias ($T_1 > T_2$), the near-field radiative heat flux exhibits exponential growth due to the convergence of the phonon linewidth of the hot terminal with that of the cold terminal.⁵³ However, in the backward direction ($T_1 < T_2$), the difference in phonon linewidth between the hot terminal and cold terminal increases, resulting in a decrease in the transmission coefficient.⁵³ Due to the increasing temperature difference, the near-field radiative heat flux continues to rise, albeit with a dampened trend. The thermal diode exhibits a maximum rectification ratio approaching 3.7 when subjected to a temperature difference of 240 K. The influence of the isotope

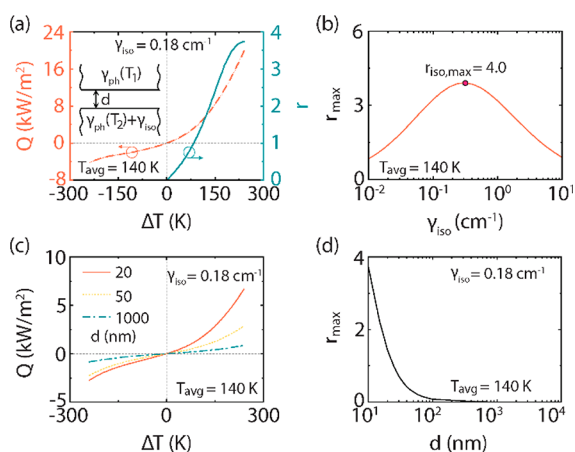


Figure 5. Isotope effect on the performance of a radiative thermal diode. (a) The net heat flux and rectification ratio with respect to the temperature difference for a radiative thermal diode. (b) The maximum rectification ratio with respect to the phonon linewidth due to isotope effect. (c) Q - ΔT curves of the thermal diode at different vacuum gap distances. (d) The maximum rectification ratio of the thermal diode with respect to vacuum gap distance. The average temperature is fixed at 140 K. The isotope concentration is added asymmetrically to one terminal of the thermal diode, which is indicated in each plot.

effect on the maximum rectification ratio is shown in Figure 5b, where the concentration of isotope enrichment can be adjusted to achieve a maximum rectification ratio of 4.0 in this thermal diode. The impact of the vacuum gap distance is illustrated in Figure 5c,d. In general, increasing the vacuum gap distance can have a detrimental effect on the rectification performance of the thermal diode. This thermal diode remains functional only when the gap distance is less than 100 nm. As indicated by other near-field thermal diodes with thin-film structure,^{37,51} the rectification ratio can be further improved, since the propagating modes are suppressed, and the surface modes dominate the radiative heat transfer. Moreover, the sensitivity of the gap distance on the performance of the NDTC devices and thermal regulators is discussed in Supporting Information. Nonetheless, the remarkable capability of isotope engineering is exemplified in the development of this thermal diode, highlighting its potential in advancing nonlinear radiative devices.

The significance of BAs in the context of these nonlinear thermal devices lies in its strongly temperature- and isotope-dependent phonon linewidth, which can greatly influence the radiative heat transfer in near-field regime. In a broader perspective, if a material exhibits a broad span of changes in its phonon linewidth due to controllable parameters (temperature, isotope concentration, or even defects), spanning several orders of magnitude, this material would be a promising candidate for realizing these nonlinear thermal devices. Such candidates could include III–V and IV semiconductor compounds (silicon carbide and boron antimonide) with a strong four-phonon scattering effect on phonon linewidth.⁵³ However, it is crucial to recognize that these nonlinear heat transfer phenomena also require other conditions, including optical phonon frequencies, phonon anharmonicity, and the temperatures of the hot and cold terminals.

In summary, we theoretically propose and demonstrate the potential of phonon scattering engineering for enabling unique nonlinear thermal radiative phenomena including NDTC

devices, thermal regulators, and thermal diodes. In particular, we propose a radiative heat flux regulator with an infinite on/off switching ratio and a tunable temperature window for a stabilized heat flux through isotope engineering. Using symmetric or asymmetric enrichment of the isotope element in the device terminals, we have successfully demonstrated the tunability of critical temperature in NDTC devices, the switching ratio of temperature regulators, and the rectification ratio of thermal diodes. These results emphasize the effectiveness of isotope and temperature engineering in achieving adjustable performance characteristics in nonlinear radiative thermal devices. Furthermore, this integration of phonon and photon science in controlling heat flux at the nanoscale holds significant promise for advancing thermal management and modulation applications.

■ ASSOCIATED CONTENT

Data Availability Statement

Data will be made available on request.

Supporting Information

The Supporting Information is available free of charge at <https://pubs.acs.org/doi/10.1021/acs.nanolett.3c03375>.

Effect of vacuum gap spacing on the performance of negative differential thermal conductance device and thermal regulator (PDF)

■ AUTHOR INFORMATION

Corresponding Author

Yiulin Ruan – School of Mechanical Engineering and the Birck Nanotechnology Center, Purdue University, West Lafayette, Indiana 47907-2088, United States; orcid.org/0000-0001-7611-7449; Email: ruan@purdue.edu

Authors

Dudong Feng – School of Mechanical Engineering and the Birck Nanotechnology Center, Purdue University, West Lafayette, Indiana 47907-2088, United States; orcid.org/0000-0002-2289-1313

Xiaolong Yang – School of Mechanical Engineering and the Birck Nanotechnology Center, Purdue University, West Lafayette, Indiana 47907-2088, United States; Present Address: X.Y.: College of Physics and Center of Quantum Materials and Devices, Chongqing University, Chongqing 401331, China

Complete contact information is available at:

<https://pubs.acs.org/10.1021/acs.nanolett.3c03375>

Notes

The authors declare no competing financial interest.

■ ACKNOWLEDGMENTS

D.F. and X.R. acknowledge partial support from the US National Science Foundation through award 2102645.

■ REFERENCES

- Wehmeyer, G.; Yabuki, T.; Monachon, C.; Wu, J.; Dames, C. Thermal diodes, regulators, and switches: Physical mechanisms and potential applications. *Applied Physics Reviews* **2017**, *4* (4), No. 041304.
- Klinar, K.; Swoboda, T.; Muñoz Rojo, M.; Kitanovski, A. Fluidic and Mechanical Thermal Control Devices. *Advanced Electronic Materials* **2021**, *7* (3), No. 2000623.

- (3) DiPirro, M. J.; Shirron, P. J. Heat switches for ADRs. *Cryogenics* **2014**, *62*, 172–176.
- (4) Du, T.; Xiong, Z.; Delgado, L.; Liao, W.; Peoples, J.; Kantharaj, R.; Chowdhury, P. R.; Marconnet, A.; Ruan, X. Wide range continuously tunable and fast thermal switching based on compressible graphene composite foams. *Nat. Commun.* **2021**, *12* (1), 4915.
- (5) Li, N.; Ren, J.; Wang, L.; Zhang, G.; Hänggi, P.; Li, B. Colloquium: Phononics: Manipulating heat flow with electronic analogs and beyond. *Rev. Mod. Phys.* **2012**, *84* (3), 1045–1066.
- (6) Ben-Abdallah, P.; Biehs, S.-A. Thermotronics: Towards Nanocircuits to Manage Radiative Heat Flux. *Zeitschrift für Naturforschung A* **2017**, *72* (2), 151–162.
- (7) Roberts, N. A.; Walker, D. G. A review of thermal rectification observations and models in solid materials. *International Journal of Thermal Sciences* **2011**, *50* (5), 648–662.
- (8) Wong, M. Y.; Tso, C. Y.; Ho, T. C.; Lee, H. H. A review of state of the art thermal diodes and their potential applications. *Int. J. Heat Mass Transfer* **2021**, *164*, No. 120607.
- (9) Li, B.; Wang, L.; Casati, G. Thermal Diode: Rectification of Heat Flux. *Phys. Rev. Lett.* **2004**, *93* (18), No. 184301.
- (10) Zhai, H.; Fan, D.; Li, Q. Dynamic radiation regulations for thermal comfort. *Nano Energy* **2022**, *100*, No. 107435.
- (11) Wei, H.; Gu, J.; Ren, F.; Zhang, L.; Xu, G.; Wang, B.; Song, S.; Zhao, J.; Dou, S.; Li, Y. Smart Materials for Dynamic Thermal Radiation Regulation. *Small* **2021**, *17* (35), No. 2100446.
- (12) Guo, R.; Shan, L.; Wu, Y.; Cai, Y.; Huang, R.; Ma, H.; Tang, K.; Liu, K. Phase-change materials for intelligent temperature regulation. *Materials Today Energy* **2022**, *23*, No. 100888.
- (13) Li, B.; Wang, L.; Casati, G. Negative differential thermal resistance and thermal transistor. *Appl. Phys. Lett.* **2006**, *88* (14), No. 143501.
- (14) Zhu, L.; Otey, C. R.; Fan, S. Negative differential thermal conductance through vacuum. *Appl. Phys. Lett.* **2012**, *100* (4), No. 044104.
- (15) Hu, J.; Wang, Y.; Vallabhaneni, A.; Ruan, X.; Chen, Y. P. Nonlinear thermal transport and negative differential thermal conductance in graphene nanoribbons. *Appl. Phys. Lett.* **2011**, *99* (11), No. 113101.
- (16) Klinar, K.; Kitanovski, A. Thermal control elements for caloric energy conversion. *Renewable and Sustainable Energy Reviews* **2020**, *118*, No. 109571.
- (17) Smyth, M.; Quinlan, P.; Mondol, J. D.; Zacharopoulos, A.; McLarnon, D.; Pugsley, A. The experimental evaluation and improvements of a novel thermal diode pre-heat solar water heater under simulated solar conditions. *Renewable Energy* **2018**, *121*, 116–122.
- (18) Muhumuza, R.; Zacharopoulos, A.; Mondol, J. D.; Smyth, M.; Pugsley, A. Experimental study of heat retention performance of thermal diode Integrated Collector Storage Solar Water Heater (ICSSWH) configurations. *Sustainable Energy Technologies and Assessments* **2019**, *34*, 214–219.
- (19) Hu, R.; Liu, Y.; Shin, S.; Huang, S.; Ren, X.; Shu, W.; Cheng, J.; Tao, G.; Xu, W.; Chen, R.; Luo, X. Emerging Materials and Strategies for Personal Thermal Management. *Adv. Energy Mater.* **2020**, *10* (17), No. 1903921.
- (20) Tang, K.; Dong, K.; Li, J.; Gordon, M. P.; Reichertz, F. G.; Kim, H.; Rho, Y.; Wang, Q.; Lin, C.-Y.; Grigoropoulos, C. P.; Javey, A.; Urban, J. J.; Yao, J.; Levinson, R.; Wu, J. Temperature-adaptive radiative coating for all-season household thermal regulation. *Science* **2021**, *374* (6574), 1504–1509.
- (21) Miao, R.; Kishore, R.; Kaur, S.; Prasher, R.; Dames, C. A non-volatile thermal switch for building energy savings. *Cell Reports Physical Science* **2022**, *3* (7), No. 100960.
- (22) Hengeveld, D. W.; Mathison, M. M.; Braun, J. E.; Groll, E. A.; Williams, A. D. Review of Modern Spacecraft Thermal Control Technologies. *HVAC&R Research* **2010**, *16* (2), 189–220.
- (23) Swanson, T. D.; Birur, G. C. NASA thermal control technologies for robotic spacecraft. *Applied Thermal Engineering* **2003**, *23* (9), 1055–1065.
- (24) Feng, D.; Yao, S.-C.; Zhang, T.; Zhang, Q. Modeling of a Smart Heat Pump Made of Laminated Thermoelectric and Electrocaloric Materials. *Journal of Electronic Packaging* **2016**, *138* (4), No. 041004.
- (25) Kittel, P. Heat switch limitations on multi-stage Magnetic Refrigeration. *AIP Conf. Proc.* **2002**, *613* (1), 1167–1174.
- (26) Sun, Y.; Hu, Y.; Shi, K.; Zhang, J.; Feng, D.; Wu, X. Negative differential thermal conductance between Weyl semimetals nanoparticles through vacuum. *Phys. Scr.* **2022**, *97* (9), No. 095506.
- (27) Dey, S. S.; Timossi, G.; Amico, L.; Marchegiani, G. Negative differential thermal conductance by photonic transport in electronic circuits. *Phys. Rev. B* **2023**, *107* (13), No. 134510.
- (28) Schmotz, M.; Maier, J.; Scheer, E.; Leiderer, P. A thermal diode using phonon rectification. *New J. Phys.* **2011**, *13* (11), No. 113027.
- (29) Kage, Y.; Hagino, H.; Yanagisawa, R.; Maire, J.; Miyazaki, K.; Nomura, M. Thermal phonon transport in Si thin film with dog-leg shaped asymmetric nanostructures. *Jpn. J. Appl. Phys.* **2016**, *55* (8), No. 085201.
- (30) Ghanekar, A.; Xiao, G.; Zheng, Y. High Contrast Far-Field Radiative Thermal Diode. *Sci. Rep.* **2017**, *7* (1), No. 6339.
- (31) Yang, Y.; Basu, S.; Wang, L. Radiation-based near-field thermal rectification with phase transition materials. *Appl. Phys. Lett.* **2013**, *103* (16), No. 163101.
- (32) Li, Q.; He, H.; Chen, Q.; Song, B. Thin-Film Radiative Thermal Diode with Large Rectification. *Physical Review Applied* **2021**, *16* (1), No. 014069.
- (33) Li, Q.; He, H.; Chen, Q.; Song, B. Radiative Thermal Diode via Hyperbolic Metamaterials. *Physical Review Applied* **2021**, *16* (6), No. 064022.
- (34) Fiorino, A.; Thompson, D.; Zhu, L.; Mittapally, R.; Biehs, S.-A.; Bezenenet, O.; El-Bondry, N.; Bansropun, S.; Ben-Abdallah, P.; Meyhofer, E.; Reddy, P. A Thermal Diode Based on Nanoscale Thermal Radiation. *ACS Nano* **2018**, *12* (6), 5774–5779.
- (35) Ito, K.; Nishikawa, K.; Miura, A.; Toshiyoshi, H.; Iizuka, H. Dynamic Modulation of Radiative Heat Transfer beyond the Blackbody Limit. *Nano Lett.* **2017**, *17* (7), 4347–4353.
- (36) Ito, K.; Nishikawa, K.; Iizuka, H.; Toshiyoshi, H. Experimental investigation of radiative thermal rectifier using vanadium dioxide. *Appl. Phys. Lett.* **2014**, *105* (25), No. 253503.
- (37) Feng, D.; Yee, S. K.; Zhang, Z. M. Near-field photonic thermal diode based on hBN and InSb films. *Appl. Phys. Lett.* **2021**, *119* (18), No. 181111.
- (38) Debernardi, A.; Baroni, S.; Molinari, E. Anharmonic Phonon Lifetimes in Semiconductors from Density-Functional Perturbation Theory. *Phys. Rev. Lett.* **1995**, *75* (9), 1819–1822.
- (39) Yang, X.; Feng, T.; Kang, J. S.; Hu, Y.; Li, J.; Ruan, X. Observation of strong higher-order lattice anharmonicity in Raman and infrared spectra. *Phys. Rev. B* **2020**, *101* (16), No. 161202.
- (40) Tong, Z.; Peoples, J.; Li, X.; Yang, X.; Bao, H.; Ruan, X. Electronic and phononic origins of BaSO₄ as an ultra-efficient radiative cooling paint pigment. *Materials Today Physics* **2022**, *24*, No. 100658.
- (41) Tong, Z.; Yang, X.; Feng, T.; Bao, H.; Ruan, X. First-principles predictions of temperature-dependent infrared dielectric function of polar materials by including four-phonon scattering and phonon frequency shift. *Phys. Rev. B* **2020**, *101* (12), No. 125416.
- (42) Han, Z.; Yang, X.; Sullivan, S. E.; Feng, T.; Shi, L.; Li, W.; Ruan, X. Raman Linewidth Contributions from Four-Phonon and Electron-Phonon Interactions in Graphene. *Phys. Rev. Lett.* **2022**, *128* (4), No. 045901.
- (43) Li, X.; Zhang, J.; Puretzky, A. A.; Yoshimura, A.; Sang, X.; Cui, Q.; Li, Y.; Liang, L.; Ghosh, A. W.; Zhao, H.; Unocic, R. R.; Meunier, V.; Rouleau, C. M.; Sumpter, B. G.; Geohagan, D. B.; Xiao, K. Isotope-Engineering the Thermal Conductivity of Two-Dimensional MoS₂. *ACS Nano* **2019**, *13* (2), 2481–2489.

- (44) Chen, S.; Wu, Q.; Mishra, C.; Kang, J.; Zhang, H.; Cho, K.; Cai, W.; Balandin, A. A.; Ruoff, R. S. Thermal conductivity of isotopically modified graphene. *Nat. Mater.* **2012**, *11* (3), 203–207.
- (45) Cardona, M.; Thewalt, M. L. W. Isotope effects on the optical spectra of semiconductors. *Rev. Mod. Phys.* **2005**, *77* (4), 1173–1224.
- (46) Matsuo, S.; Makita, T. Isotope effect on the viscosity of benzene and cyclohexane mixtures under high pressures. *Int. J. Thermophys.* **1993**, *14* (1), 67–77.
- (47) Slack, G. A. Effect of Isotopes on Low-Temperature Thermal Conductivity. *Phys. Rev.* **1957**, *105* (3), 829–831.
- (48) Berman, R.; Foster, E. L.; Ziman, J. M.; Simon, F. E. The thermal conductivity of dielectric crystals: the effect of isotopes. *Proceedings of the Royal Society of London. Series A. Mathematical and Physical Sciences* **1956**, 237 (1210), 344–354.
- (49) Xie, L.; Song, B. Isotope effect on radiative thermal transport. *Phys. Rev. B* **2023**, *107* (13), No. 134308.
- (50) Mittapally, R.; Lim, J. W.; Zhang, L.; Miller, O. D.; Reddy, P.; Meyhofer, E. Probing the Limits to Near-Field Heat Transfer Enhancements in Phonon-Polaritonic Materials. *Nano Lett.* **2023**, *23* (6), 2187–2194.
- (51) Xie, L.; Song, B. Isotope engineering of near-field radiative thermal diodes. *Int. J. Heat Mass Transfer* **2023**, *214*, No. 124377.
- (52) Zhang, Z. M. *Nano/microscale heat transfer*; Springer Nature: Cham, 2020.
- (53) Feng, D.; Yang, X.; Han, Z.; Ruan, X. Four phonon-dominated near-field radiation in weakly anharmonic polar materials. *arXiv*, Sept. 29, 2023, ver. 1. DOI: [10.48550/arXiv.2309.17344](https://doi.org/10.48550/arXiv.2309.17344).
- (54) Feng, T.; Lindsay, L.; Ruan, X. Four-phonon scattering significantly reduces intrinsic thermal conductivity of solids. *Phys. Rev. B* **2017**, *96* (16), No. 161201.
- (55) Feng, T.; Ruan, X. Quantum mechanical prediction of four-phonon scattering rates and reduced thermal conductivity of solids. *Phys. Rev. B* **2016**, *93* (4), No. 045202.
- (56) Tamura, S.-i. Isotope scattering of dispersive phonons in Ge. *Phys. Rev. B* **1983**, *27* (2), 858–866.